Alkali-Resistant Catalysts

DOI: 10.1002/anie.201205808

A "Smart" Hollandite DeNO$_x$ Catalyst: Self-Protection against Alkali Poisoning**

*Zhiwei Huang, Xiao Gu, Wen Wen, Pingping Hu, Michiel Makkee, He Lin, Freek Kapteijn, and Xingfu Tang**

Global warming, caused by an increase in atmospheric CO_2 concentrations, and limited fossil-fuel resources have stimulated the search for environmentally sustainable energy sources with zero or low CO_2 emission.[1] The use of biomass as a CO_2-neutral fuel has drawn widespread attention, since biomass as part of the global carbon ecocycle is an increasingly important energy resource.[2] An associated issue, which is often encountered in the control of NO_x emissions from the alkali-rich stack gas of power plants (co-)fuelled by biomass, is the severe deactivation of conventional V_2O_5-WO_3/TiO_2 catalysts in the selective catalytic reduction of NO by NH_3 (NH_3-SCR).[3,4] This deactivation is predominately caused by the strong interaction of alkali-metal ions with catalytically active sites.[4–11] For example, Zheng et al.[8] proposed a deactivation mechanism by proton exchange at catalytically active Brønsted acid sites with alkali-metal ions. The exchange reactions occur readily at normal NH_3-SCR operating temperatures because alkali species, such as KCl and K_2SO_4, are mobile in view of their low Tamman temperatures (T_{Tam}).[12]

On the basis of this deactivation mechanism, a possible approach to the development of an alkali-resistant catalyst is to increase the number of catalytically active sites and "alkali-active" sites (for trapping alkalis), for example, by using a support with the property of high or super acidity or by increasing the concentration of active elements.[9–11,13,14] However, this approach can not completely alleviate alkali poisoning because, to a great extent, alkali-metal ions and reactants compete for the same sites. Therefore, the development of a highly alkali resistant catalyst remains a great challenge. Herein we describe the successful development of a hollandite manganese oxide (HMO) catalyst with separate catalytically active sites (for NH_3-SCR) and alkali-active sites (for alkali trapping). With the combined action of the two types of active sites, this bifunctional HMO catalyst not only protects catalytically active sites against alkali poisoning, but also preserves high catalytic activity at the original level until all the alkali-active sites are occupied.

We used K^+ as a probe to clearly identify the catalytically active sites of HMO in NH_3-SCR reactions, as K^+ is a well-known catalyst poison.[7–11] Figure 1 shows the catalytic activity of HMO with different K^+ loadings in NH_3-SCR reactions at 350 °C as expressed in terms of the rate constant for the conversion of NO.[9–11] The K^+ loading had almost no influence on the catalytic activity of HMO, and all HMO catalysts tested exhibited almost the same activity.

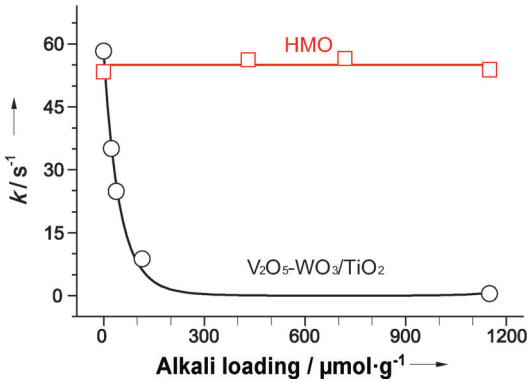

Figure 1. Rate constant (k) for the conversion of NO as a function of alkali loading for HMO and V_2O_5-WO_3/TiO_2. Catalytic tests were conducted at a normal NH_3-SCR reaction temperature of 350 °C (1000 ppm NO, 1000 ppm NH_3, 3 % O_2, balance N_2) with a gas hourly space velocity (GHSV) of 40 000 h^{-1}. The alkali loading corresponds to the molar content of the alkali-metal ion with respect to the weight of the HMO or the V_2O_5-WO_3/TiO_2 catalyst (μmol g^{-1}). The catalysts were annealed at 400 °C after alkali loading.

For reference, a conventional deNO$_x$ catalyst (V_2O_5-WO_3/TiO_2) with different K^+ loadings was also tested in the NH_3-SCR reactions under the same conditions (Figure 1). As expected, the V_2O_5-WO_3/TiO_2 catalyst exhibited rather poor alkali resistance and underwent severe and continuous deactivation with increasing alkali loadings until complete loss of activity was observed: the catalytic activity strongly decreased as the K^+ loading was increased from 0 to 100 μmol g^{-1}, and the catalyst was almost completely deactivated when the alkali loading exceeded 200 μmol g^{-1}. The results indicate that the deactivation of the catalyst predominantly originates from the occupation of the catalytically active sites by K^+, as corroborated by previous reports.[4–8] In other words, the catalytically active sites and the "alkali-active" sites of the V_2O_5-WO_3/TiO_2 catalyst are identical.

[*] Z. Huang, Dr. X. Gu, P. Hu, Prof. X. Tang
Department of Environmental Science and Engineering
Fudan University, Shanghai, 200433 (China)
E-mail: tangxf@fudan.edu.cn
Dr. W. Wen, Dr. H. Lin
Shanghai Synchrotron Radiation Facility
Chinese Academy of Sciences, Shanghai, 201204 (China)
Prof. M. Makkee, Prof. F. Kapteijn
Catalysis Engineering, Delft University of Technology
Delft, 2628 BL (The Netherlands)

[**] This research was supported financially by the NSFC (20977018, 21077026, and 21277032) and the NBRPC (2010CB934501).
Supporting information for this article is available on the WWW under http://dx.doi.org/10.1002/anie.201205808.

In contrast, HMO exhibited excellent alkali resistance. Even at an extraordinarily high K^+ loading of 1150 μmol g^{-1}, the catalytic activity of HMO was the same as that of the V_2O_5-WO_3/TiO_2 catalyst with a K^+ loading of 23 μmol g^{-1}. Thus, the alkali resistance of HMO is theoretically 50 times higher than that of conventional catalysts under identical conditions. When the alkali loading was below 1150 μmol g^{-1}, the alkali-metal ion, the counterion in the salt used, and the alkali loading had almost no influence on the catalytic performance of HMO in a wide NH_3-SCR temperature window of 200–350 °C (see Figures S1–S3 in the Supporting Information), whereas these factors generally have a crucial influence on the catalytic activities of catalysts (see Figure S4).[4,5,7,15] The experimental evidence supports the hypothesis that HMO has two separate types of active sites: catalytically active sites and "alkali-active" sites.

Although we could ascertain that HMO had different types of sites, their location was not clear. For NH_3-SCR reactions, neither O_2 (one of the reactants) nor N_2 (one of the products) fits in the tunnels of HMO, as the diameters of O_2 (3.46 Å) and N_2 (3.64 Å) are much larger than that of the effective pore opening (ca. 2.65 Å).[16] Therefore, the NH_3-SCR reactions must only take place at the external surface of the HMO nanorods and not in the tunnels.

The external surfaces of HMO include the side facets and the {001} top facets (see Figure S5):[17] which of these contain the catalytically active sites? For HMO with different K^+ loadings, there are different amounts of K^+ on the {001} facets (see Figure S6 and the related discussion in Section 2.1 of the Supporting Information). As the K^+ loading has no influence on the catalytic activity of HMO, the {001} facets do not appear to comprise the catalytically active sites, in analogy with our results in a recent study.[18] Moreover, when the HMO catalyst is overloaded with K^+ beyond the maximum capacity of HMO (1280 μmol g^{-1}; see the related calculation in Section 2.2 of the Supporting Information), that is, when the catalytically active sites on the {110} facets of HMO also become occupied by K^+ (see Figure S7), the catalytic activity decreases dramatically (see Figure S3). Therefore, we can conclude that the exposed {110} side facets of the HMO nanorods contain the catalytically active sites in the NH_3-SCR reactions.

To investigate the active sites for alkali storage in HMO, we initially supported KCl as a typical alkali source on the external surface of HMO. The resulting sample KCl/HMO was annealed at 400 °C to give a material referred to as K-HMO. Both KCl particles and HMO nanorods were observed in the TEM and high-resolution TEM (HRTEM) images of KCl/HMO (Figure 2a,b). In contrast, the KCl particles are absent in K-HMO: smooth surfaces were observed in the (HR)TEM images (Figure 2c; see also Figure S8). However, the presence of potassium species in/on K-HMO was shown by elemental mapping by energy-dispersive X-ray spectroscopy (EDX) in conjunction with the corresponding scanning transmission electron microscopy (STEM) image (Figure 2d). A K/Mn molar ratio obtained by EDS for K-HMO (see Figure S9) is close to the K/Mn molar ratio found for KCl/HMO by X-ray fluorescence elemental analysis. The chlorine content is 3.1 wt% in KCl/HMO but negligible for K-HMO

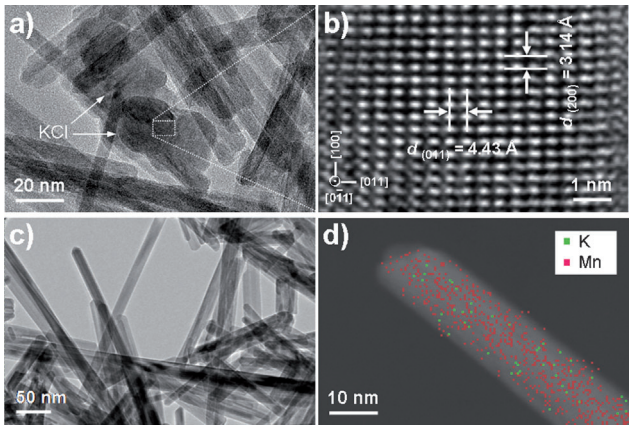

Figure 2. a) TEM image of KCl/HMO. b) HRTEM image of the KCl particle indicated in (a) as viewed along an [0-11] axis of the KCl crystal. c) TEM image of K-HMO. d) Bright-field STEM image of an individual K-HMO nanorod with the corresponding elemental mapping by EDX.

(see Table S1). It was demonstrated that HCl gas is produced from KCl/HMO during thermal processing (see Figure S10 and Section 2.3 of the Supporting Information). Consequently, it was clear that K^+ had been inserted in the internal tunnels of HMO through ion-exchange reactions with the tunnel protons, with the release of HCl gas.[12]

The location of the alkali-active sites in HMO was further confirmed by room-temperature synchrotron X-ray diffraction (XRD) patterns (see Figure S11). The reflections of HMO as a function of momentum transfer, Q, can be indexed as the hollandite manganese oxide with a tetragonal structure (JCPDS 44-0141).[19,20] The reflections of both KCl and HMO appear in the XRD pattern of KCl/HMO. The intensity and the Bragg position of the HMO reflections remained almost unchanged after loading with KCl, which indicates that crystalline KCl is present at the external surface of HMO and is consistent with the corresponding TEM image (Figure 2a). After annealing, the reflections of KCl vanished in the XRD pattern of K-HMO, and no new reflections appeared. These observations indicated the presence of highly dispersed K^+. To identify alkali-active sites, we compared the intensity and the position of the reflections for K-HMO and HMO. All reflection intensities were greater for K-HMO, except those for the (211), (600), and (002) planes, which remained almost unchanged (see Figures S7 and S11). Thus, by considering the influence of structural factors on the diffraction intensity,[19] we concluded that K^+ occupied the (0,0,0) sites of the crystal structure of HMO. The appearance of the (200) and (002) Bragg reflections of K-HMO at lower and higher Bragg angles, respectively, in comparison with those of HMO (see Figure S12) indicates an expansion of the *a* lattice axis and a contraction of the *c* axis. The evidence strongly supports the occupation of the (0,0,0) sites of the HMO crystal structure by K^+ after the annealing of KCl/HMO, in analogy with related structures.[19–21] Therefore, the internal tunnels of HMO are the "alkali-active" sites.

All characterization data discussed above provide evidence for the existence of two types of separate active sites in

HMO: alkali-active sites located in the internal tunnels for trapping alkali-metal ions and catalytically active sites located at the {110} side facets of the external surface for catalyzing the NH_3-SCR reaction.

In a biomass-fuelled boiler, combustion of the biomass (e.g. straw or wood) results in stack gas with fly-ash particles in the sub-micrometer range. These particles have a high content of potassium compounds (especially KCl), which can poison the catalytically active sites through surface migration or mobility to the active sites.[22,23] In practice, if the catalyst is exposed to the stack gas, alkali-metal ions are initially accumulated at the external surface of the catalyst, whereas the alkali-active sites of HMO are located in the internal tunnels. To determine whether alkali-metal ions can spontaneously migrate from the external surface into the tunnels of HMO and liberate the catalytically active sites for the NH_3-SCR reaction, we conducted an experiment to simulate the exposure of catalysts to the NH_3-SCR environment at a biomass power plant.

We conducted successive NH_3-SCR reactions over KCl/HMO (which has a structure similar to that resulting from the initial accumulation of KCl on the surface of HMO catalyst) to investigate the combined effect of the two types of active sites of HMO. We examined the conversion of NO over KCl/HMO and HMO (see Figure S13) and plotted the activity of KCl/HMO in terms of the turnover frequency (TOF; see Section 2.4 of the Supporting Information) against time for two consecutive reactions over the same catalyst (Figure 3a). In the first run, the reaction was carried out according to a temperature-programmed procedure at a ramp rate of 5 °C min^{-1} from 50 to 350 °C; the reaction reached a steady state at 350 °C. The TOF profile involved three stages: In the first stage, the TOF value strongly increased with increasing temperature up to about 230 °C. In the second stage, above 230 °C, the TOF value sharply decreased to about 0.2×10^{-3} s^{-1} until the final temperature of 350 °C was reached. In the third isothermal stage, the reaction rate gradually increased and reached a steady level with a TOF value of approximately 1.5×10^{-3} s^{-1}. After this run, the catalyst was cooled down to 50 °C, and the second reaction was carried out by the same procedure. In the first stage, the development of the TOF profile was similar to that observed for the first run below 230 °C. In the second stage, the TOF value only decreased to approximately 1.5×10^{-3} s^{-1}, the steady-state level in run 1, and remained at this level in the third stage. Thus, stages two and three were quite different from the corresponding stages in the first run.

To shed light on the essential discrepancy of the above two consecutive runs, we carried out temporal in situ synchrotron XRD analysis of KCl/HMO as a function of temperature (Figure 3b; see also Figures S14 and S15). The XRD pattern of KCl/HMO at 40 °C is similar to the room-temperature XRD pattern (see Figure S11). When the temperature was increased to about 230 °C, the intensity of the Bragg reflection of the KCl gradually decreased, and the reflection location shifted to smaller Bragg angles. When the temperature was increased further, the KCl reflections vanished, in good agreement with the fact that when the T_{Tam} value of KCl is reached (T_{Tam} = 230 °C for the KCl particles in this case), the

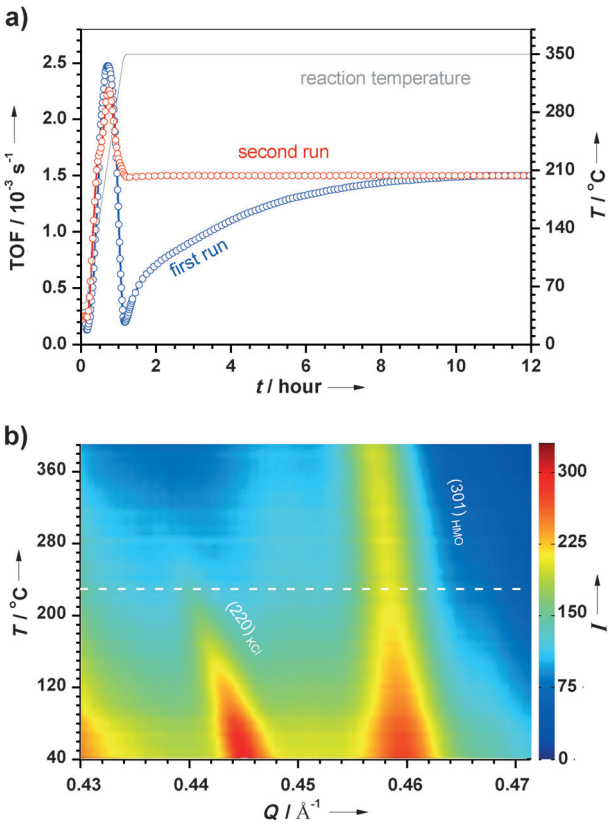

Figure 3. a) TOF profiles with time (t) on stream for KCl/HMO with a K^+ loading of 1150 μmol g^{-1} in two consecutive NH_3-SCR reactions. After the first reaction, the catalyst was cooled to 50 °C. Catalytic tests were conducted with a GHSV of 80000 h^{-1} (1000 ppm NO, 1000 ppm NH_3, 3% O_2, balance N_2, ramp rate: 5 °C min^{-1}). b) Contour map of the temporal in situ synchrotron XRD patterns of KCl/HMO in a temperature range of 40–390 °C with a ramp rate of 5 °C min^{-1}. The diffraction intensities (I) of the $(220)_{KCl}$ reflection of KCl and the $(301)_{HMO}$ reflection of HMO are shown as a function of temperature (T).

atoms of the bulk KCl become mobile.[12] The tetragonal hollandite crystal structure essentially remained unchanged during the whole process, except for slight changes in the intensity and the location of the reflections. No new reflections appeared, and the XRD pattern was similar to the room-temperature pattern of K-HMO (see Figure S11). All the evidence presented above strongly supports the conclusion that K^+ spontaneously migrates from the blocked catalytically active surface sites into the internal tunnel space of HMO at temperatures above the T_{Tam} value of the KCl particles.

We conducted density functional theoretical calculations on the K^+ diffusion process. The diffusion path of K^+ possibly involves three steps (Figure 4): in the first step, a K^+ ion on the {110} side facet migrates to the border near the {001} top facet (from A to B); in the second step, it crosses the boundary onto the {001} top facet (the mouth of the tunnel nearest to the {110} side facet, from B to C); and in the third step, it migrates into the tunnel (from C to D). It is relatively easy for the K^+ ion to migrate from the {110} side facet onto the {001} top facet, since the energy barrier in each case is only

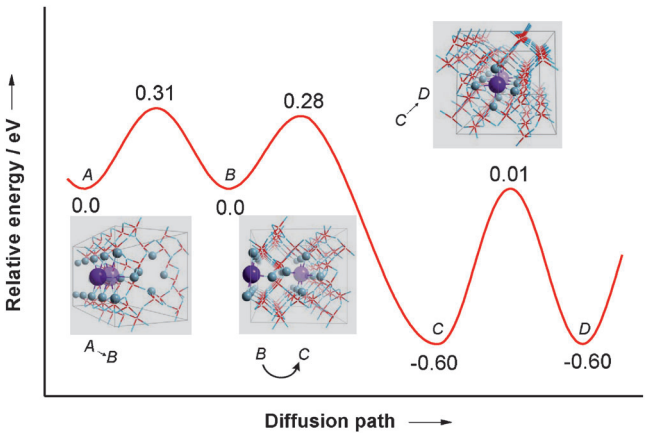

Figure 4. Possible diffusion path of a K^+ ion on the surface and into a tunnel of HMO. The local minimum equilibrium positions are denoted by *A*, *B*, *C*, and *D*.

about 0.3 eV. Although a higher energy barrier (0.61 eV) needs to be overcome for migration from the {001} top facet into the tunnel, the ballistic migration of the K^+ ion into the internal tunnels is also easy, because the absolute energy barrier is only 0.01 eV for this migration with respect to the total energy of the K^+ ion on the {110} side facet, in analogy with reported results.[24] Therefore, from an energetic point of view, it is not difficult for the K^+ ion to migrate from the {110} side facets into the internal tunnels across the {001} top facets.

The temporal in situ synchrotron XRD patterns coupled with the theoretical calculations give a good interpretation of the combined effect of the two types of active sites of HMO in the NH_3-SCR reaction. In the first run, the TOF rapidly increases as the reaction temperature is increased in the first stage (Figure 3a). This behavior implies that the majority of the catalytically active sites of HMO are not occupied by K^+ ions, since the migration of KCl does not occur. In the second stage of the first run, the almost complete loss of activity indicates the poisoning of the catalytically active sites by the K^+ ions as a result of their surface migration/mobility. In the third stage, the K^+ ions continuously migrate into the internal tunnels and release the catalytically active sites. Activity is gradually recovered and finally reaches a steady-state level when all K^+ ions have completely migrated into the tunnels. In the second run, the TOF remains at a steady level in the isothermal third stage because the migration of K^+ ions is complete after the first run. The initial activity decrease in both second stages is attributed to the desorption of NH_3 and/or the consumption of surface species (e.g. $-NH_2$, $-NH_4^+$).[25,26] These processes decrease the surface concentration of NH_3. Overall, our results show that under normal NH_3-SCR conditions, alkalis can spontaneously migrate from the catalytically active surface sites into the internal tunnels; thus, the HMO catalyst can protect itself from alkali poisoning.

An average accumulation rate of alkali-metal ions on the surface of catalysts has been evaluated to be approximately 4.2×10^{-2} μmol g^{-1} h^{-1} at a normal biomass power plant,[27] and the conventional V_2O_5-WO_3/TiO_2 catalyst was deactivated by more than 75% after only 1500 h on stream.[28] According to these parameters, the lifetime of HMO can be extrapolated to be approximately 25000 h (about three years) if we assume a capacity for alkali accumulation of 1150 μmol g^{-1} and that alkali poisoning is the only mode of deactivation under practical conditions. We anticipate that high alkali resistance is not unique to hollandite manganese oxide catalysts, but that any other metal oxide with a hollandite structure with unoccupied tunnels (for example, hollandite titanium oxides,[29] cryptomelane,[30] priderite,[31] and akaganéite[32]) should exhibit similar high alkali resistance. Thus, catalysts with a hollandite structure show promise for application at power plants (co-)fuelled by biomass.

In summary, it has been demonstrated that an HMO NH_3-SCR catalyst possesses two types of active sites: catalytically active sites on the external surface and alkali-trapping sites in the internal tunnels, which account for its strong resistance against alkali poisoning. Alkalis accumulated on the catalytically active surface sites of HMO can spontaneously migrate into the internal tunnels under normal reaction conditions. Owing to this self-protection function, catalysts with a hollandite structure should enable the environmentally friendly use of biomass in energy generation.

Received: July 23, 2012
Revised: October 21, 2012
Published online: November 22, 2012

Keywords: alkali metals · biomass · catalytically active sites · heterogeneous catalysis · manganese oxide

[1] R. Slade, R. Gross, A. Bauen, *Energy Environ. Sci.* **2011**, *4*, 2645.
[2] A. Faaij, *Energy Policy* **2006**, *34*, 322.
[3] B. Sander, *Biomass Bioenergy* **1997**, *12*, 177.
[4] Y. J. Zheng, A. D. Jensen, J. E. Johnsson, *Ind. Eng. Chem. Res.* **2004**, *43*, 941.
[5] J. P. Chen, R. T. Yang, *J. Catal.* **1990**, *125*, 411.
[6] J. Due-Hansen, S. Boghosian, A. Kustov, P. Fristrup, G. Tsilomelekis, K. Stahl, C. H. Christensen, R. Fehrmann, *J. Catal.* **2007**, *251*, 459.
[7] H. Kamata, K. Takahashi, C. Odenbrand, *J. Mol. Catal. A* **1999**, *139*, 189.
[8] Y. J. Zheng, A. D. Jensen, J. E. Johnsson, *Appl. Catal. B* **2005**, *60*, 253.
[9] S. Putluru, A. Riisager, R. Fehrmann, *Appl. Catal. B* **2011**, *101*, 183.
[10] S. Putluru, A. D. Jensen, A. Riisager, R. Fehrmann, *Top. Catal.* **2011**, *54*, 1286.
[11] S. Putluru, S. B. Kristensen, J. Due-Hansen, A. Riisager, R. Fehrmann, *Catal. Today* **2012**, *184*, 192.
[12] J. A. Moulijn, A. E. Van-Diepen, F. Kapteijn, *Appl. Catal. A* **2001**, *212*, 3.
[13] S. Putluru, A. D. Jensen, A. Riisager, R. Fehrmann, *Catal. Sci. Technol.* **2011**, *1*, 631.
[14] S. B. Kristensen, A. J. Kunov-Kruse, A. Riisager, S. B. Rasmussen, R. Fehrmann, *J. Catal.* **2011**, *284*, 60.
[15] O. Kröcher, M. Elsener, *Appl. Catal. B* **2008**, *77*, 215.
[16] Z. M. Wang, S. Tezuka, H. Kanoh, *Chem. Mater.* **2001**, *13*, 530.
[17] Z. W. Huang, X. Gu, Q. Q. Cao, P. P. Hu, J. M. Hao, J. H. Li, X. F. Tang, *Angew. Chem.* **2012**, *124*, 4274; *Angew. Chem. Int. Ed.* **2012**, *51*, 4198.
[18] C. Wang, L. Sun, Q. Q. Cao, B. Q. Hu, Z. W. Huang, X. F. Tang, *Appl. Catal. B* **2011**, *101*, 598.

[19] B. Dawson, *Proc. R. Soc. London Ser. A* **1967**, *298*, 255.
[20] J. Vicat, E. Fanchon, P. Strobel, D. T. Qui, *Acta Crystallogr. Sect. B* **1986**, *42*, 162.
[21] Y. Tanaka, M. Tsuji, Y. Tamaura, *Phys. Chem. Chem. Phys.* **2000**, *2*, 1473.
[22] A. Kling, C. Andersson, A. Myringer, D. Eskilsson, S. G. Jaras, *Appl. Catal. B* **2007**, *69*, 240.
[23] Y. J. Zheng, P. A. Jensen, A. D. Jensen, B. Sander, H. Junker, *Fuel* **2007**, *86*, 1008.
[24] M. Witko, R. Grybos, R. Tokarz-Sobieraj, *Top. Catal.* **2006**, *38*, 105.
[25] F. Kapteijn, L. Singoredjo, M. Vandriel, A. Andreini, J. A. Moulijn, G. Ramis, G. Busca, *J. Catal.* **1994**, *150*, 105.
[26] P. P. Hu, Z. W. Huang, W. M. Hua, X. Gu, X. F. Tang, *Appl. Catal. A* **2012**, *437–438*, 139.
[27] F. Castellino, A. D. Jensen, J. E. Johnsson, R. Fehrmann, *Appl. Catal. B* **2009**, *86*, 206.
[28] C. Andersson, C. U. I. Odenbrand, L. H. Andersson, *Värmeforsk* **1998**, 646.
[29] C. Y. Xu, Q. Zhang, H. Zhang, L. Zhen, J. Tang, L. C. Qin, *J. Am. Chem. Soc.* **2005**, *127*, 11584.
[30] J. Cai, J. Liu, W. S. Willis, S. L. Suib, *Chem. Mater.* **2001**, *13*, 2413.
[31] J. E. Post, R. B. Vondreele, P. R. Buseck, *Acta Crystallogr. Sect. B* **1982**, *38*, 1056.
[32] J. Cai, J. Liu, Z. Gao, A. Navrotsky, S. L. Suib, *Chem. Mater.* **2001**, *13*, 4595.

